Chiral Interactions up to Next-to-Next-to-Next-to-Leading Order and Nuclear Saturation

C. Drischler,[1,2,*] K. Hebeler,[1,2,†] and A. Schwenk[1,2,3,‡]
[1]Institut für Kernphysik, Technische Universität Darmstadt, 64289 Darmstadt, Germany
[2]ExtreMe Matter Institute EMMI, GSI Helmholtzzentrum für Schwerionenforschung GmbH, 64291 Darmstadt, Germany
[3]Max-Planck-Institut für Kernphysik, Saupfercheckweg 1, 69117 Heidelberg, Germany

(Received 25 October 2017; revised manuscript received 16 August 2018; published 28 January 2019)

We present an efficient Monte Carlo framework for perturbative calculations of infinite nuclear matter based on chiral two-, three-, and four-nucleon interactions. The method enables the incorporation of all many-body contributions in a straightforward and transparent way, and makes it possible to extract systematic uncertainty estimates by performing order-by-order calculations in the chiral expansion as well as the many-body expansion. The versatility of this new framework is demonstrated by applying it to chiral low-momentum interactions, exhibiting a very good many-body convergence up to fourth order. Following these benchmarks, we explore new chiral interactions up to next-to-next-to-next-to-leading order (N^3LO). Remarkably, simultaneous fits to the triton and to saturation properties can be achieved, while all three-nucleon low-energy couplings remain natural. The theoretical uncertainties of nuclear matter are significantly reduced when going from next-to-next-to-leading order to N^3LO.

DOI: 10.1103/PhysRevLett.122.042501

Introduction.—Recent calculations of medium-mass and heavy nuclei have demonstrated the importance of realistic saturation properties of infinite matter for nuclear forces derived within chiral effective field theory (EFT) [1–5]. While most nucleon-nucleon (NN) and three-nucleon (3N) interactions fitted to only two- and few-body observables are able to predict light nuclei in agreement with experimental data, the theoretical uncertainties tend to increase with increasing mass number $A \gtrsim 16$ (see, e.g., Ref. [6]) and significant discrepancies to experiment can be found for properties of heavy nuclei [7]. There have been efforts to include properties of heavier nuclei in the optimization of chiral nuclear forces [1]. Such interactions tend to exhibit more realistic saturation properties of nuclear matter and also show improved agreement with experiment for energies and radii of medium-mass and heavy nuclei [2,8–10]. However, the explicit incorporation of nuclear matter properties in the optimization process of nuclear forces has not been feasible so far due to the computational complexity of such calculations.

Nuclear matter has been studied based on chiral NN and 3N interactions within coupled-cluster theory [11], quantum Monte Carlo methods [12–14], the self-consistent Green's function method [15], and many-body perturbation theory (MBPT) [16–24]. The advantages of MBPT are its computational efficiency as well as the possibility to estimate many-body uncertainties by comparing results at different orders. So far, MBPT for infinite matter has only been applied up to third order including also the particle-hole channels [20,24], where N^2LO 3N contributions beyond Hartree-Fock have been included as normal-ordered two-body interactions [22,25,26]. Normal ordering allows to incorporate 3N operators in form of lower-body operators [27], and nuclear-structure calculations show that this is an excellent approximation for softer chiral interactions (see, e.g., Refs. [28,29]). In the MBPT expansion around Hartree Fock this is a very natural approximation, as the reference state is sufficiently close to the ground state. There remain however significant challenges, especially regarding the role of higher-order particle-hole vs. particle-particle or hole-hole contributions as well as the inclusion of next-to-next-to-next-to-leading order (N^3LO) 3N interactions beyond Hartree-Fock [18,23].

Novel framework.—In this Letter, we present a new Monte Carlo framework for MBPT, which is tailored to address these challenges. We perform our calculations directly in a single-particle product basis $|\mathbf{k}_i\sigma_i\tau_i\rangle$, without needing involved partial-wave decompositions. Tracing over spin $|\sigma_i\rangle$ and isospin states $|\tau_i\rangle$ of each particle with label i is fully automated, whereas the multidimensional integrals over the momenta $\mathbf{k}_i$ are computed using adaptive Monte Carlo algorithms [30–32]. This makes implementing arbitrary energy diagrams straightforward (including particle-hole contributions), even up to high orders in MBPT, while approximations in normal ordering are not needed anymore. However, it is well known that the number of diagrams at each order increases rapidly, with 3, 39, and 840 at third, fourth, and fifth order for NN-only interactions [33,34]. Within our Monte Carlo framework, a manual implementation of these would be feasible but still tedious and at least inefficient. We therefore developed an automatic C++ code generator based on the analytic expression of a given diagram.

In addition, we developed a general method to represent chiral interactions exactly as matrices in spin-isospin space, where the matrix elements are analytic functions of the single-particle momenta $\mathbf{k}_i$ in the programming language C++. The automated generation of these interaction matrices is close to the operatorial definition of chiral forces [35–43], which we implemented with nonlocal regulators up to N^{3}LO. For the incorporation of NN interactions whose operatorial structure is not directly accessible (e.g., renormalization-group evolved potentials), we sum the contributions from all partial-wave channels for each Monte Carlo sampling point.

Specifically, in this first application, we consider all contributions from NN interactions up to fourth order in MBPT (around the Hartree-Fock reference state). Contributions from 3N interactions are included exactly up to second order, including residual 3N-3N terms, which have only been evaluated so far for contact interactions [44]. At third order, we neglect all terms that involve at least one residual 3N contribution, whereas at fourth order we neglect all 3N contributions. These contributions turn out to be smaller (see discussion below). This amounts to 4, $20 = 3 \times 2^3 - 4$, and $24 = 39 - 15$ diagrams at second, third, and fourth order, respectively, with up to 21-dimensional momentum integrals per diagram. The number of diagrams at third (fourth) order can be reduced by 4 (15) at zero temperature. In comparison, a full calculation would involve $39 \times 2^4 = 624$ fourth-order diagrams.

We assess the numerical convergence of the integration by varying the number of sampling points as well as employing two different Monte Carlo algorithms [31], in addition to the variance as statistical uncertainty. The framework is remarkably efficient due to performance optimization and parallelization. Most diagrams up to fourth order can be evaluated within about 10 min to a precision of $\lesssim$10 keV. The precise evaluation of a few specific third-order diagrams involving three 3N interactions requires more time due to the higher dimensionality of the momentum integrals. However, the precision can be controlled in a systematic way when short runtimes are important, e.g., for optimizing nuclear interactions. Finally, we have performed detailed benchmarks against third-order results in the literature (see Supplemental Material [45]), including for the dilute Fermi gas [46] and semianalytical as well as partial-wave-based MBPT calculations [24,47].

Results for nuclear matter.—In Fig. 1 we present results for the energy per particle in symmetric nuclear matter and neutron matter based on the Hebeler+ [16] and NNLOsim [6] NN and 3N interactions up to fourth order in MBPT. For symmetric matter we show the empirical saturation region by a gray box with boundaries $n_0 = 0.164 \pm 0.007\,\mathrm{fm}^{-3}$ and $E/A = -15.86 \pm 0.37 \pm 0.2\,\mathrm{MeV}$, where the first uncertainty is as in Ref. [22] and we add

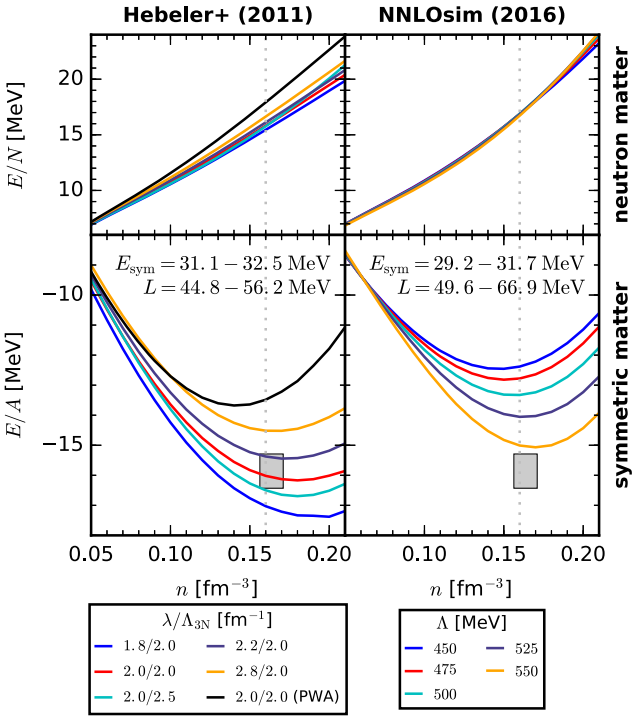

FIG. 1. Energy per particle of neutron matter (top row) and symmetric nuclear matter (bottom row) based on the Hebeler+ [16] and NNLOsim [6] NN and 3N interactions (columns). Results are shown for λ/Λ_{3N} for the interactions of Ref. [16] and $\Lambda = \Lambda_{NN,3N}$ for those of Ref. [6].

0.2 MeV from Ref. [48]. We also give results for the symmetry energy $E_{\mathrm{sym}} = E/N - E/A$ as well as its slope parameter $L = 3n_0\partial_n E_{\mathrm{sym}}$ at $n_0 = 0.16$ fm^{-3} (dashed vertical line). Both are predicted with narrow ranges.

The Hebeler+ interactions [16] were obtained by a similarity renormalization group evolution [27] of the N^{3}LO NN potential of Ref. [49] to different resolution scales λ, whereas the two leading-order 3N couplings c_D (one-pion-exchange contact interaction) and c_E (3N contact interaction) were fixed at these resolution scales by fits to the ^{3}H binding energy and the ^{4}He charge radius for two different 3N cutoffs Λ_{3N}. Note that these potentials include NN (N^{3}LO) and 3N forces (N^{2}LO) up to different orders in the chiral expansion. Despite being fitted to only few-body data, these interactions are able to reproduce empirical saturation in Fig. 1 within uncertainties given by the spread of the individual Hebeler+ interactions [16]. In addition, recent calculations of medium-mass to heavy nuclei based on some of these interactions show remarkable agreement with experiment [2,4,8–10,50] and thus offer new *ab initio* possibilities to investigate the nuclear chart.

The second column of Fig. 1 shows results for the NNLOsim potentials [6] ($T_{\mathrm{lab}}^{\mathrm{max}} = 290$ MeV) for different cutoff values (see legend). These interactions were obtained by a simultaneous fit of all low-energy couplings to two-body and few-body data for $\Lambda_{NN} = \Lambda_{3N}$. We observe a

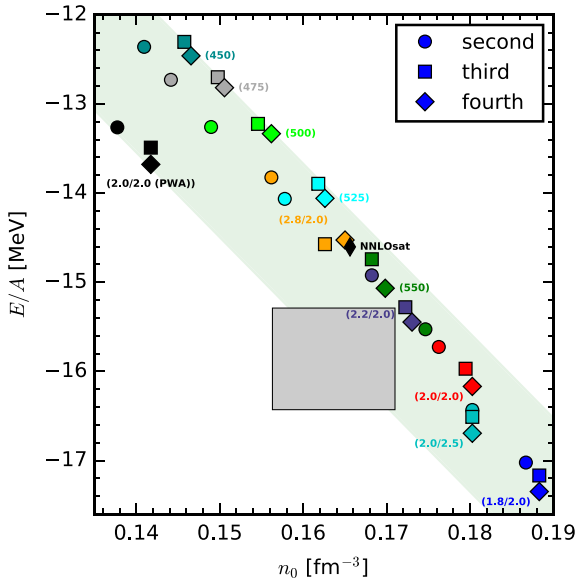

FIG. 2. Correlation between the calculated saturation density n_0 and saturation energy E/A for the Hebeler+ [16] and NNLOsim [6] NN and 3N interactions obtained at second, third, and fourth order in MBPT. The values of λ/Λ_{3N} and $\Lambda_{NN} = \Lambda_{3N}$, as well as the saturation region are as in Fig. 1. The diamond refers to the NNLOsat result [1].

weak cutoff dependence for these potentials in neutron matter over the entire density range and in symmetric matter up to $n \lesssim 0.08$ fm^{-3}. At higher densities, the variation of the energy per particle increases up to ~3 MeV at $n_0 = 0.16$ fm^{-3} with a very similar density dependence. Overall, all the NNLOsim interactions turn out to be too repulsive compared to the empirical saturation region.

We study the many-body convergence of the Hebeler+ and NNLOsim interactions by plotting in Fig. 2 the calculated saturation energy as a function of the calculated saturation density at second, third, and fourth order in MBPT. The annotated values denote the cutoff scales of the different potentials (see legend of Fig. 1). For all low-momentum interactions as well as with $\Lambda \leq 525$ MeV, we observe a very good convergence in the many-body expansion, indicating that these chiral interactions are perturbative over this density regime. Moreover, we find a pronounced linear correlation similar to the Coester line [51]. In contrast to the original Coester line with NN potentials only, the green band encompassing all (fourth-order) saturation points in Fig. 2 overlaps with the empirical saturation region because of the inclusion of 3N forces. Notice, however, that no point lies within the gray box. Note also that the Hebeler+ interaction that breaks most from the linear correlation is "2.0/2.0 (PWA)," for which the c_i values in the 3N forces are larger than in the NN part [16].

Finally, in Table I we show the hierarchy of contributions from second, third, and fourth order at $n_0 = 0.16$ fm^{-3} for the Hebeler+ "1.8/2.0" interaction, which is most commonly used in the recent *ab initio* calculations of medium-mass and heavy nuclei. At second order, we give the contributions from NN interactions (NN-only), from NN plus 3N contributions that can be represented in form of a density-dependent NN interaction (NN + 3N), and the residual 3N contribution (3N res.). We find that the residual 3N term is significantly smaller compared to the other contributions. Furthermore, we find that the third-order contributions are significantly smaller than the second-order terms for all studied interactions. These findings suggest that the studied interactions exhibit a natural MBPT convergence pattern for a cutoff of 450 MeV, whereas we already find first indications of a reduced convergence rate for $\Lambda = 500$ MeV. Additional higher-order implementations will, however, be necessary to draw final conclusions on the convergence.

Fit to saturation region.—The observed convergence pattern indicates that the studied unevolved nonlocal interactions with $\Lambda \leq 525$ MeV are sufficiently perturbative and allow calculations with controlled many-body uncertainties. This offers the possibility to use the new Monte Carlo framework for constraining the 3N couplings using information from nuclear matter. In this Letter, we demonstrate this using the N^{2}LO and N^{3}LO NN potentials

TABLE I. Contributions to the energy per particle at $n_0 = 0.16$ fm^{-3} in symmetric nuclear matter at consecutive orders in MBPT based on the Hebeler+ [16] interaction with $\lambda/\Lambda_{3N} = 1.8/2.0$ fm^{-1} and the N^{2}LO and N^{3}LO interactions of this work with Λ/c_D [for the central c_D fit value (black diamonds) in Fig. 3]. All energies are in MeV.

		Second order			Third order	Fourth order	
Chiral order	Λ/c_D	NN-only	NN + 3N	3N res.	NN + 3N	NN-only	NN + 3N[a]
N^{3}LO/N^{2}LO	$\lambda/\Lambda_{3N} = 1.8/2.0$ fm^{-1}	−2.30	−2.54	−0.10	−0.10	−0.20	−0.07
N^{2}LO	450/ + 2.50	−6.23	−13.38	−0.42	−2.08	0.07	0.24
	500/ − 1.50	−8.61	−14.49	−0.66	−0.77	0.32	0.75
N^{3}LO	450/ + 0.25	−8.84	−14.52	−0.32	−2.28	0.61	1.03
	500/ − 2.75	−10.56	−14.98	−0.83	−1.05	0.65	1.14

[a]Contributions from 3N forces at fourth order in MBPT are not included in our fits. The values here are an uncertainty estimate using normal-ordered 3N contributions in the $P = 0$ approximation, where the center-of-mass momentum of the effective two-body potential is set to zero [22,25].

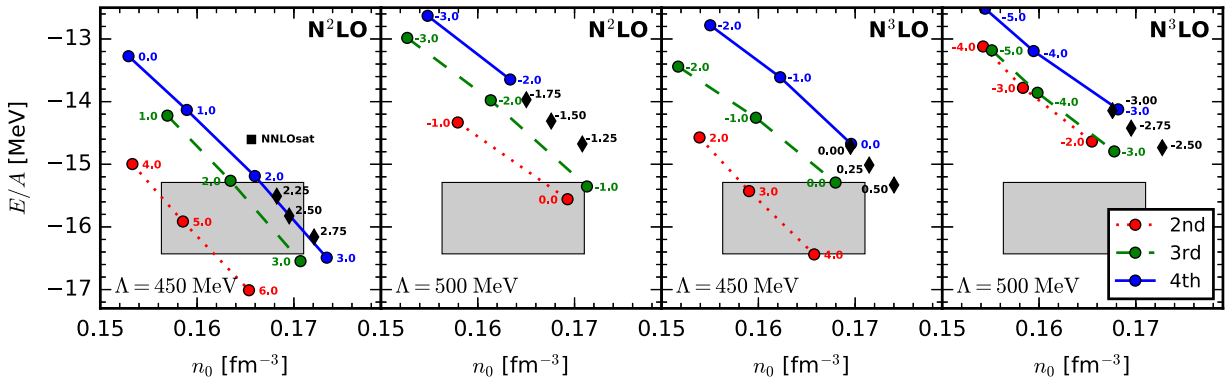

FIG. 3. Saturation density and energy of symmetric nuclear matter at different orders in MBPT for the NN and 3N interactions at N^{2}LO and N^{3}LO. The points are for different values of c_D (annotated numbers; c_E follows from Fig. 1 of the Supplemental Material [45]), while the red-dotted, green-dashed, and blue-solid lines correspond to calculations at second, third, and fourth order in MBPT. The left (right) two panels are for N^{2}LO (N^{3}LO) with $\Lambda = 450$ and 500 MeV. The diamonds in each panel represent the calculations with a simultaneous good reproduction of both saturation density and energy at fourth order.

of Entem, Machleidt, and Nosyk (ENM) [43] with $\Lambda_{\rm NN} = 450$ and 500 MeV, which are also very promising in terms of their Weinberg eigenvalues [52]. As a first step, we fit to the ^{3}H binding energy that leads to a relation of the 3N couplings c_D and c_E (shown in Fig. 1 of the Supplemental Material [45]). For the fits, we include all 3N contributions consistently up to N^{2}LO and N^{3}LO, respectively. The corresponding 3N matrix elements were computed as in Ref. [53]. We use $\Lambda = \Lambda_{\rm NN,3N}$ and a nonlocal regulator of the form $f_\Lambda(p,q) = \exp[-((p^2 + 3/4q^2)/\Lambda_{\rm 3N}^2)^4]$ for the Jacobi momenta p and q of the initial and final states [36]. For both cutoffs and chiral orders, we obtain c_E couplings of natural size in the wide c_D range explored.

As a second step, we calculate nuclear matter for the range of 3N couplings and determine the saturation point. In Fig. 3, we present the saturation points at N^{2}LO and N^{3}LO as a function of c_D and at different orders in MBPT. Similar to the interactions shown in Fig. 2, we find a natural convergence pattern. Note that the shown points on the trajectories correspond to different c_D values at second order compared to third and fourth order. Contributions at third order are therefore more significant in these cases, whereas fourth-order corrections are again much smaller as is shown in Table I (the convergence at fixed densities is documented in Table I of the Supplemental Material [45]). In general, Fig. 3 demonstrates that it is possible to determine natural c_D/c_E combinations at N^{2}LO and N^{3}LO with good saturation properties for both cutoff cases considered. However, N^{3}LO contributions provide slightly too much repulsion.

In each panel of Fig. 3, we mark the three couplings that provide a good fit to the saturation region by black diamonds, with annotated c_D values (the corresponding c_E values are given in Fig. 1 of the Supplemental Material [45]). The resulting equations of state of symmetric nuclear matter and neutron matter at N^{2}LO and N^{3}LO are shown in Fig. 4. Note that only two lines are present in neutron matter since the shorter-range 3N interactions do not contribute [25]. We also calculate the Hartree-Fock energy of the N^{3}LO 4N forces using the nonlocal regulator as in Ref. [18]. These forces are long range and free of unknown

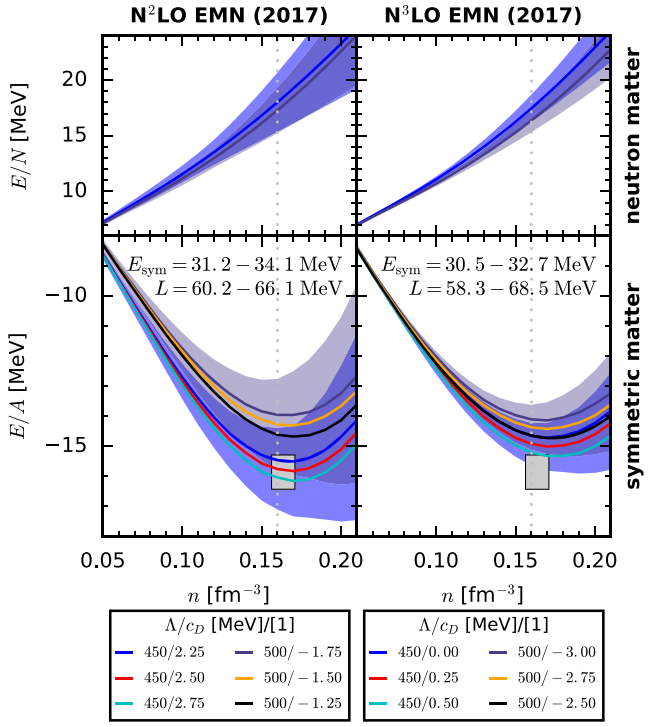

FIG. 4. Energy per particle in neutron matter (top row) and symmetric nuclear matter (bottom row) based on chiral interactions at N^{2}LO (first column) and N^{3}LO (second column) fit to the empirical saturation region (see Fig. 3). The fits are labeled by Λ/c_D in the legend. The blue ($\Lambda = 450$ MeV) and gray ($\Lambda = 500$ MeV) bands estimate the theoretical uncertainty following Ref. [42]. Note that the annotated results for $E_{\rm sym}$ and L do not include this uncertainty.

parameters [39,40]. The obtained 4N Hartree-Fock energies at n_0 are $\approx -(150\text{–}200)$ keV in neutron matter as well as symmetric matter, in agreement with the results of Ref. [18]. As for the Hebeler+ and NNLOsim results, the symmetry energy and the L parameter are predicted with a remarkably narrow range. In symmetric matter, we also observe a weak cutoff dependence at N^{3}LO, whereas the results for $\Lambda = 450$ MeV are clearly separated from $\Lambda = 500$ MeV at N^{2}LO, with the former achieving the best fits to the saturation region. Finally, we estimate the theoretical uncertainty from the chiral expansion following Ref. [42], using $Q = p/\Lambda_b$ with breakdown scale $\Lambda_b = 500$ MeV and average momentum $p = \sqrt{3/5}k_{\mathrm{F}}$. The bands overlap from N^{2}LO to N^{3}LO, and we clearly see that the uncertainties are significantly reduced at N^{3}LO. For reference, results at LO and NLO are shown in Fig. 2 of the Supplemental Material [45].

Summary.—We have presented a new Monte Carlo framework for calculations of nuclear matter, which allows us to include higher-order contributions from chiral interactions and is capable of going to high enough orders in the many-body expansion for suitable interactions. The new method was applied to the calculation of the symmetric-matter and neutron-matter energy in an expansion around Hartree-Fock, but it can be easily generalized to expansions around other reference states. This enabled first benchmarks of chiral low-momentum interactions to fourth order in MBPT showing a systematic order-by-order convergence. We then used this to develop new chiral interactions at N^{2}LO and N^{3}LO, including NN, 3N, and 4N interactions at N^{3}LO, where the 3N couplings are fit to the triton and to saturation properties. Our work shows that a good description of nuclear matter at these orders is possible, with a systematic behavior from N^{2}LO to N^{3}LO and natural low-energy couplings. Thanks to the computational efficiency, the new framework is also ideal for the incorporation of nuclear matter properties in the fitting of novel nuclear interactions. It will be exciting to see what these interactions predict for nuclei and for the equation of state for astrophysics.

We thank A. Ekström, B. Carlsson, C. Forssén, R. J. Furnstahl, and T. Hahn for useful discussions, R. Machleidt for providing us with the EMN potentials, and J. W. Holt for benchmark values at third order in MBPT. We also thank C. Iwainsky for helping us to optimize the code performance. This work was supported in part by the European Research Council Grant No. 307986 STRONGINT and the Deutsche Forschungsgemeinschaft through Grant SFB 1245. Computational resources have been provided by the Lichtenberg high performance computer of the TU Darmstadt.

*christian.drischler@physik.tu-darmstadt.de
†kai.hebeler@physik.tu-darmstadt.de
‡schwenk@physik.tu-darmstadt.de

[1] A. Ekström, G. R. Jansen, K. A. Wendt, G. Hagen, T. Papenbrock, B. D. Carlsson, C. Forssén, M. Hjorth-Jensen, P. Navrátil, and W. Nazarewicz, Phys. Rev. C **91**, 051301(R) (2015).
[2] G. Hagen, A. Ekström, C. Forssén, G. R. Jansen, W. Nazarewicz, T. Papenbrock, K. A. Wendt, S. Bacca, N. Barnea, B. Carlsson, C. Drischler, K. Hebeler, M. Hjorth-Jensen, M. Miorelli, G. Orlandini, A. Schwenk, and J. Simonis, Nat. Phys. **12**, 186 (2016).
[3] J. Simonis, K. Hebeler, J. D. Holt, J. Menéndez, and A. Schwenk, Phys. Rev. C **93**, 011302(R) (2016).
[4] J. Simonis, S. R. Stroberg, K. Hebeler, J. D. Holt, and A. Schwenk, Phys. Rev. C **96**, 014303 (2017).
[5] A. Ekström, G. Hagen, T. D. Morris, T. Papenbrock, and P. D. Schwartz, Phys. Rev. C **97**, 024332 (2018).
[6] B. D. Carlsson, A. Ekström, C. Forssén, D. F. Strömberg, G. R. Jansen, O. Lilja, M. Lindby, B. A. Mattsson, and K. A. Wendt, Phys. Rev. X **6**, 011019 (2016).
[7] S. Binder, J. Langhammer, A. Calci, and R. Roth, Phys. Lett. B **736**, 119 (2014).
[8] R. F. Garcia Ruiz *et al.*, Nat. Phys. **12**, 594 (2016).
[9] G. Hagen, G. R. Jansen, and T. Papenbrock, Phys. Rev. Lett. **117**, 172501 (2016).
[10] T. D. Morris, J. Simonis, S. R. Stroberg, C. Stumpf, G. Hagen, J. D. Holt, G. R. Jansen, T. Papenbrock, R. Roth, and A. Schwenk, Phys. Rev. Lett. **120**, 152503 (2018).
[11] G. Hagen, T. Papenbrock, A. Ekström, K. Wendt, G. Baardsen, S. Gandolfi, M. Hjorth-Jensen, and C. J. Horowitz, Phys. Rev. C **89**, 014319 (2014).
[12] A. Gezerlis, I. Tews, E. Epelbaum, S. Gandolfi, K. Hebeler, A. Nogga, and A. Schwenk, Phys. Rev. Lett. **111**, 032501 (2013).
[13] A. Roggero, A. Mukherjee, and F. Pederiva, Phys. Rev. Lett. **112**, 221103 (2014).
[14] J. E. Lynn, I. Tews, J. Carlson, S. Gandolfi, A. Gezerlis, K. E. Schmidt, and A. Schwenk, Phys. Rev. Lett. **116**, 062501 (2016).
[15] A. Carbone, A. Polls, and A. Rios, Phys. Rev. C **88**, 044302 (2013).
[16] K. Hebeler, S. K. Bogner, R. J. Furnstahl, A. Nogga, and A. Schwenk, Phys. Rev. C **83**, 031301(R) (2011).
[17] I. Tews, T. Krüger, K. Hebeler, and A. Schwenk, Phys. Rev. Lett. **110**, 032504 (2013).
[18] T. Krüger, I. Tews, K. Hebeler, and A. Schwenk, Phys. Rev. C **88**, 025802 (2013).
[19] J. W. Holt, N. Kaiser, and W. Weise, Prog. Part. Nucl. Phys. **73**, 35 (2013).
[20] L. Coraggio, J. W. Holt, N. Itaco, R. Machleidt, L. E. Marcucci, and F. Sammarruca, Phys. Rev. C **89**, 044321 (2014).
[21] C. Wellenhofer, J. W. Holt, N. Kaiser, and W. Weise, Phys. Rev. C **89**, 064009 (2014).
[22] C. Drischler, K. Hebeler, and A. Schwenk, Phys. Rev. C **93**, 054314 (2016).
[23] C. Drischler, A. Carbone, K. Hebeler, and A. Schwenk, Phys. Rev. C **94**, 054307 (2016).
[24] J. W. Holt and N. Kaiser, Phys. Rev. C **95**, 034326 (2017).
[25] K. Hebeler and A. Schwenk, Phys. Rev. C **82**, 014314 (2010).

[26] J. W. Holt, N. Kaiser, and W. Weise, Phys. Rev. C **81**, 024002 (2010).
[27] S. K. Bogner, R. J. Furnstahl, and A. Schwenk, Prog. Part. Nucl. Phys. **65**, 94 (2010).
[28] G. Hagen, T. Papenbrock, D. J. Dean, A. Schwenk, A. Nogga, M. Włoch, and P. Piecuch, Phys. Rev. C **76**, 034302 (2007).
[29] R. Roth, S. Binder, K. Vobig, A. Calci, J. Langhammer, and P. Navrátil, Phys. Rev. Lett. **109**, 052501 (2012).
[30] G. P. Lepage, J. Comput. Phys. **27**, 192 (1978).
[31] T. Hahn, Comput. Phys. Commun. **168**, 78 (2005).
[32] T. Hahn, Comput. Phys. Commun. **207**, 341 (2016).
[33] P. D. Stevenson, Int. J. Mod. Phys. C **14**, 1135 (2003).
[34] N. J. A. Sloane, The Encyclopedia of integer sequences: Number of labeled Hugenholtz diagrams with n nodes, https://oeis.org/A064732.
[35] R. Machleidt and D. R. Entem, Phys. Rep. **503**, 1 (2011).
[36] E. Epelbaum, A. Nogga, W. Glöckle, H. Kamada, U.-G. Meißner, and H. Witała, Phys. Rev. C **66**, 064001 (2002).
[37] V. Bernard, E. Epelbaum, H. Krebs, and U.-G. Meißner, Phys. Rev. C **77**, 064004 (2008).
[38] V. Bernard, E. Epelbaum, H. Krebs, and U.-G. Meißner, Phys. Rev. C **84**, 054001 (2011).
[39] E. Epelbaum, Phys. Lett. B **639**, 456 (2006).
[40] E. Epelbaum, Eur. Phys. J. A **34**, 197 (2007).
[41] E. Epelbaum, H. Krebs, and U.-G. Meißner, Phys. Rev. Lett. **115**, 122301 (2015).
[42] E. Epelbaum, H. Krebs, and U.-G. Meißner, Eur. Phys. J. A **51**, 53 (2015).
[43] D. R. Entem, R. Machleidt, and Y. Nosyk, Phys. Rev. C **96**, 024004 (2017).
[44] N. Kaiser, Eur. Phys. J. A **48**, 58 (2012).
[45] See Supplemental Material at http://link.aps.org/supplemental/10.1103/PhysRevLett.122.042501 for details on the c_D, c_E fits, additional benchmarks, LO and NLO results, as well as many-body convergence.
[46] H.-W. Hammer and R. J. Furnstahl, Nucl. Phys. **A678**, 277 (2000).
[47] A. Dyhdalo, R. J. Furnstahl, K. Hebeler, and I. Tews, Phys. Rev. C **94**, 034001 (2016).
[48] G. F. Bertsch and D. Bingham, Phys. Rev. Lett. **119**, 252501 (2017).
[49] D. R. Entem and R. Machleidt, Phys. Rev. C **68**, 041001(R) (2003).
[50] J. Birkhan, M. Miorelli, S. Bacca, S. Bassauer, C. A. Bertulani, G. Hagen, H. Matsubara, P. von Neumann-Cosel, T. Papenbrock, N. Pietralla, V. Y. Ponomarev, A. Richter, A. Schwenk, and A. Tamii, Phys. Rev. Lett. **118**, 252501 (2017).
[51] F. Coester, S. Cohen, B. Day, and C. M. Vincent, Phys. Rev. C **1**, 769 (1970).
[52] J. Hoppe, C. Drischler, R. J. Furnstahl, K. Hebeler, and A. Schwenk, Phys. Rev. C **96**, 054002 (2017).
[53] K. Hebeler, H. Krebs, E. Epelbaum, J. Golak, and R. Skibinski, Phys. Rev. C **91**, 044001 (2015).